Rapid Communications

Femtosecond x-ray diffraction can discern nonthermal from thermal melting

N. Medvedev,[1,2,*] M. Kopecky,[2] J. Chalupsky,[2] and L. Juha[1,2]
[1]*Institute of Plasma Physics CAS, v.v.i., Za Slovankou 3, 182 00 Prague, Czech Republic*
[2]*Institute of Physics CAS, v.v.i., Na Slovance 2, 182 21 Prague, Czech Republic*

(Received 26 January 2019; published 15 March 2019)

We theoretically investigate which experimental observations enable discrimination between thermal and nonthermal melting in femtosecond laser pulse-irradiated semiconductors. We identify that coherent phonon excitation, visible in the oscillations of various diffraction peaks, provides an opportunity to observe ongoing modifications of interatomic potential. Decoupling the effects of anharmonicity, caused by thermal heating, from the effects of evolution of the interatomic potential, due to electronic excitation, potentially enables differentiation between the two damage channels.

DOI: 10.1103/PhysRevB.99.100303

The phenomenon of ultrafast melting, which later acquired the name of nonthermal melting, has been observed in femtosecond laser pulse-irradiated covalently bonded semiconductors [1,2]. The experimental observation of a few-hundred femtosecond melting has been plausibly explained as a result of the changes of the interatomic potential surface due to high electronic excitation [3,4]. Laser-induced lattice instability is thus thought to be a result of the potential energy of the electronic system. A detailed summary of the original observations of nonthermal phenomena is given in Ref. [5].

Alternatively, the exchange of the kinetic energy between electrons and the lattice could lead to thermal melting, i.e., heating of atoms above the melting point inducing disordering in the system. Such a process lasts at the timescales of electron-phonon (or, more generally, electron-ion) coupling, which typically requires a few picoseconds [6].

It has been suggested, e.g., in [7], that an enhanced electron-phonon energy exchange could be responsible for the ultrafast melting observed in experiments. Despite a dubious theoretical basis, such suggestions raised a valid point of concern, i.e., could the two damage channels, thermal and nonthermal, be unambiguously distinguished from one another experimentally [8,9]?

So far, the nonthermal nature of ultrafast melting was only inferred from the timescales of the observed material changes [8,10,11]. Such considerations, together with the solid theoretical basis [3,12,13], make for a strong case. However, the possibility of direct discrimination between the processes involved is still lacking. In this work, we suggest that a direct observation with x-ray pump/x-ray probe has the capability to directly distinguish between the two kinds of processes and help to settle the ongoing debate. With the advent of x-ray free-electron lasers (XFELs) supporting pump-probe techniques, the proposed type of experiment has become feasible [14,15].

In this work, we used the recently developed hybrid code X-ray-induced Thermal And Nonthermal Transitions (XTANT [16]) to study theoretically transient kinetics in XFEL irradiated silicon. XTANT is capable of tracing nonequilibrium evolution of high-energy electron cascades starting from photoabsorption, Auger decays, impact ionizations, and quasielastic electron scattering (fraction of electrons out of equilibrium); low-energy electron-ion coupling; changes in the electron band structure and atomic potential energy surface; atomic motion and phase transitions; and changes in optical properties [16]. Using this model, it was previously demonstrated that upon XFEL irradiation, silicon can undergo both kinds of phase transitions [13]: (a) for an absorbed dose above $\sim$0.65 eV/atom, Si melts thermally due to electron-ion coupling; (b) for an absorbed doses above $\sim$0.9 eV/atom, silicon melts nonthermally due to modification of the atomic potential energy surface by excited electrons from the bonding valence orbitals to antibonding conduction states. This shows that XFEL excited Si is an ideal study case for a comparative investigation attempting to untangle the contributions of both effects.

We selected irradiation parameters corresponding to the expected parameters of the European XFEL [17], namely, a photon energy of 24 keV, pulse duration of $\sim$50 fs FWHM, and fluences sufficient to trigger either of the above-mentioned phase transitions in a single shot. First, we start by analyzing transient processes that take place at such high photon energies. Excitation of silicon after an XFEL irradiation starts with photoabsorption, which promotes electrons into high-energy states [18]. The fraction of such electrons with respect to the total number of the valence-band electrons in unexcited Si is shown in Fig. 1. One can see that the increase of the high-energy electron density takes place after the XFEL pulse has finished, and then decreases after $\sim$150 fs. This is due to the fact that the majority of electrons are excited via impact ionization. The photoelectron only serves as a seed, which initiates the electron cascade. This effect delays energy deposition into the low-energy electrons populating the bottom of the conduction band and forming interatomic

*Corresponding author: nikita.medvedev@fzu.cz

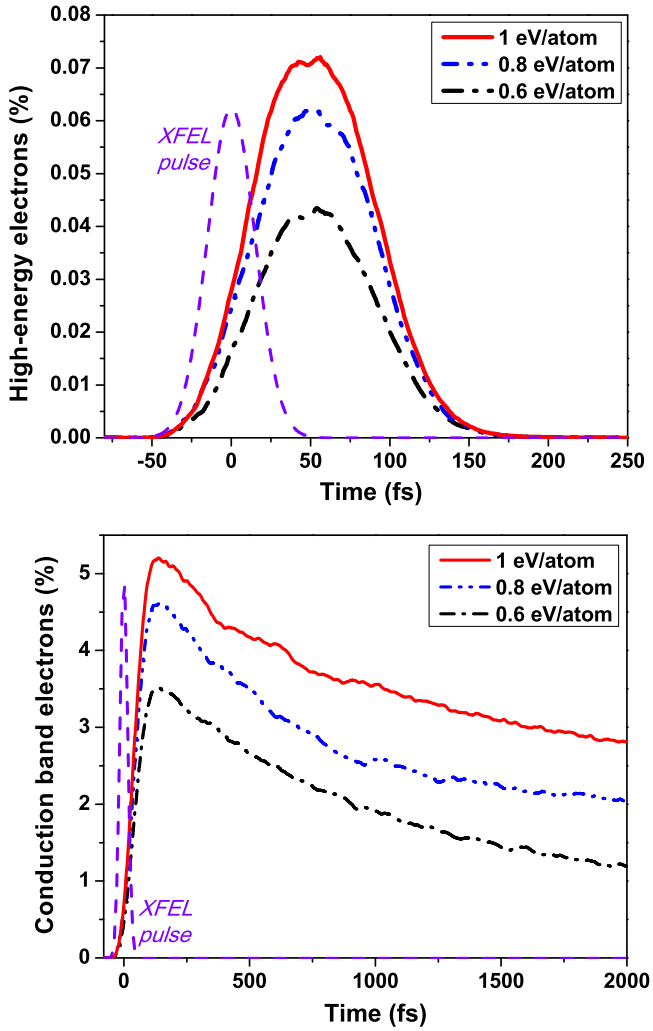

FIG. 1. Percentage of high-energy electrons (energy >10 eV, top panel) and low-energy electrons (energy <10 eV, bottom panel) in silicon exposed to a 50 fs (FWHM) laser pulse of 24 keV radiation at different absorbed doses.

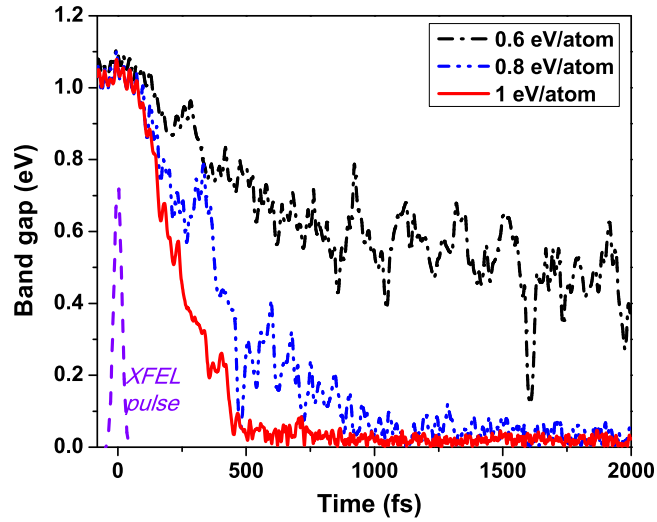

FIG. 2. Modeled band gap in silicon exposed to a 50 fs (FWHM) laser pulse of 24 keV radiation at different absorbed doses.

bonds. Qualitatively, such a delay was observed experimentally, albeit at different XFEL parameters [15]. However, this stage of electron cascade does not alter the nature of the phase transition, as is discussed below.

High-energy excited electrons deliver energy into the low-energy fraction of electrons within the valence and the bottom of the conduction band (with energies <10 eV counted from the bottom of the conduction band). The fraction of such electrons is shown in Fig. 1, which demonstrates that for the lowest modeled dose of 0.6 eV/atom, below the estimated thermal damage threshold, the density of excited electrons is nonetheless high, with ∼3.5% at its maximum reached by the end of ionization cascade (∼150−200 fs). Furthermore, the density decreases due to cooling down via electron-ion coupling. A decreasing electron temperature leads to a smaller and smaller fraction of excited electrons being present in the conduction band.

For an absorbed dose of 0.8 eV/atom, thermal melting is induced in silicon [13,19]. The electron density in Fig. 1 reaches a maximum at about ∼4.5%. This density is insufficient to trigger nonthermal melting; however, it is sufficiently high to raise the question as to what is the contribution of the modified interatomic potential to the thermal damage. This effect, at below damaging fluences, is known as phonon softening; see, e.g., [20,21].

For an absorbed dose of 1 eV/atom, the maximum electron density reaches over 5%, which is sufficient to trigger nonthermal melting with a contribution of the thermal heating of atoms [13,19].

As was discussed in previous works [13,19,22], the band-gap collapse in covalently bonded semiconductors indicates a phase transition into a metallic phase. The timescales of the band-gap collapse are indicative of nonthermal melting occurring within 300–500 fs for a dose of 1 eV/atom, as seen in Fig. 2. These timescales are a little prolonged with respect to the XUV irradiation; cf. Refs. [13,19]. Timescales over 1 ps for a dose of 0.8 eV/atom suggest thermal melting; and there is no collapse for a dose of 0.6 eV/atom corresponding to a dose which is below the damage threshold. In addition, these oscillations are observed at the sub-ps scale. As is shown below, these oscillations reflect the behavior of atomic structure.

Temperatures of the low-energy fraction of electrons after irradiation with the discussed doses peak at about 10 to 12 kK, and then reduce due to coupling into the lattice; see Fig. 3. Correspondingly, the atomic temperature increases up to 1800–2000 K, approximately the melting temperature of silicon, almost identically in all cases. It is worth noting that the electronic temperature decreases faster at higher maximal temperatures (the electron temperature curves intersect in Fig. 3). This reflects the nonlinear behavior of the electron-ion coupling parameter as a function of the electronic and atomic temperatures in silicon, as discussed in Ref. [19].

Theoretically, it is now clear that a dose of 1 eV/atom triggers a nonthermal phase transition as the melting takes place within a relatively cold lattice, i.e., at lattice temperatures below the melting point, as has been discussed in the literature [9,13]. Let us now consider what experimental observations could validate this prediction. We calculated the femtosecond

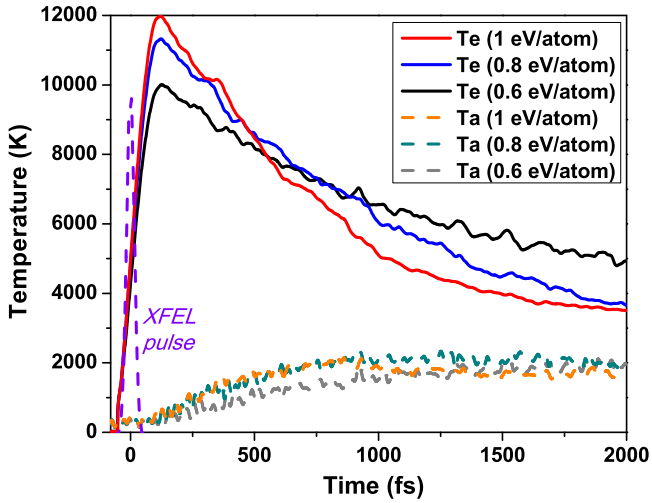

FIG. 3. Temperature of electrons and atoms in silicon exposed to a 50 fs (FWHM) laser pulse of 24 keV radiation at different absorbed doses.

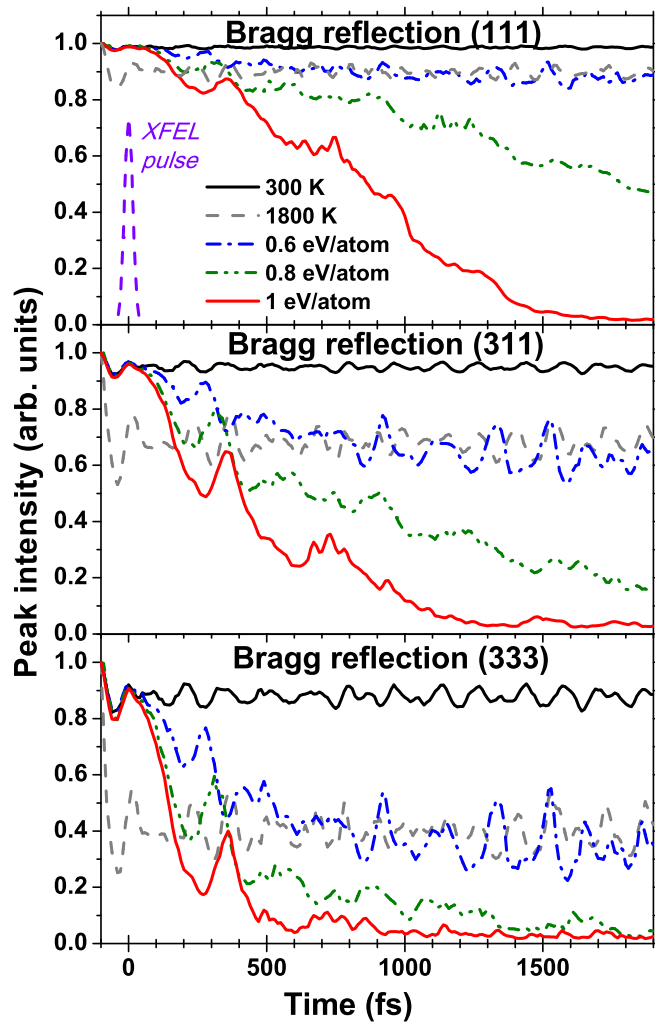

FIG. 4. Bragg peaks (111) (top panel), (311) (middle panel), and (333) (bottom panel), in silicon exposed to a 50 fs (FWHM) laser pulse of 24 keV radiation at different absorbed doses. For comparison, peaks of nonirradiated silicon at room temperature and at 1800 K are shown.

diffraction patterns, as expected from an x-ray pump/x-ray probe scheme at an XFEL.

Figure 4 shows the evolution of the Bragg peaks (111), (311), and (333) in silicon after irradiation; in addition, peaks of nonirradiated silicon at room temperature and at 1800 K (close to melting) are shown for comparison. First, we note that a comparison of the period of oscillations seen in the diffraction peak's intensity for the room and elevated atomic temperatures (300 vs 1800 K) shows that a ∼120 fs period stretches to ∼130 fs. Such a change indicates anharmonicity of the interatomic potential, without significant electronic excitation. Any changes beyond that would be indicative of the modification of the potential induced by high levels of electronic excitation described above.

For irradiated cases, one can observe a presence of strong oscillations in the Bragg reflections. They are a result of an excitation of coherent phonons by the femtosecond laser pulse [23–25]. For a 0.6 eV/atom absorbed dose, the oscillation period is about 170 fs. We can see a difference of 40 fs from the high-temperature equilibrium case (1800 K discussed above), despite nearly identical atomic temperatures (cf. Fig. 3). A high electronic temperature (and high number of excited electrons in the conduction band, ∼3.5%; see Fig. 1) causes this additional change. This effect is known as a phonon squeezing precursor to nonthermal melting [20].

For the case of a 0.8 eV/atom absorbed dose, the oscillations exhibit a more complex character, with an approximate periodicity of ∼280 fs. This stretching of the oscillations indicates that the electronic excitation softens the interatomic potential to a large degree and even below nonthermal melting. The amplitudes of these oscillations decrease with time, and such phonon damping indicates that melting is occurring in the material.

At a dose of 1 eV/atom, the oscillations are most pronounced, with their initial period of ∼350 fs. A noticeable feature in this case is that the period of oscillations lengthens over time where the next oscillation is already ∼370−400 fs and is broadened. The third oscillation is barely noticeable at 1.3−1.5 ps, with a period of ∼500−700 fs, and then completely vanishing. At even higher deposited doses, oscillations would completely vanish quicker, leading to atomic disorder.

Comparing the results of the three deposited doses, it is clearly seen that for the same atomic but different electronic temperatures, the oscillations of the Bragg peaks have different periods, i.e., they lengthen with increasing dose. Such an effect is a clear signature of nonthermal modifications of interatomic potential due to electronic excitation.

Note also that interestingly, oscillations observed in Fig. 4 resemble oscillations of the band gap in Fig. 2. Thus, experimental methods accessing the band-gap evolution over time might also be used to distinguish between thermal and nonthermal melting, although indirectly. This must be validated in dedicated experiments by simultaneously measuring coherent phonon dynamics.

Another important observation is that different Bragg peaks are disappearing at different times in both cases, i.e., nonthermal as well as thermal melting. Thus, an event of

nonconcerted disappearance of diffraction peaks cannot be used as a signature of nonthermal melting, as was suggested in [8], i.e., femtosecond laser pulse-induced thermal melting also exhibits a nonconcerted decrease in diffraction peaks.

In order to experimentally distinguish between thermal and nonthermal melting, time-resolved x-ray diffraction (tXRD) can be employed. As follows from the above summarized theory, keeping track of intensity variations at particular Bragg reflections should answer this question since an increasing period of oscillations is correlated with (nonthermal) interatomic potential softening. It has been shown that coherent phonon excitations with an FEL pulse are observable experimentally, and it is indeed possible to infer a shape of interatomic potential from them [26]. This requires a sufficiently precise single-color pump-and-probe measurement, which would monitor intensity variations in the probe beam as a function of time delay and dose deposited by the pump pulse. An x-ray free-electron laser is the most appropriate candidate for such an experiment since it provides sufficiently high intensities, photon energies, and homogeneous irradiation (to exclude transport effects) by means of ultrashort laser pulses.

Current designs of split-and-delay devices integrated or to be integrated into FEL beam lines provide temporal resolution sufficient for the characteristic timescales of nonthermal melting [27–30]. Dedicated FEL beam lines enable tXRD measurements in wide-angle x-ray scattering (WAXS) geometry accessing high-index Bragg reflections and enabling noncollinear x-ray pump and x-ray probe measurements while both beams are focused on the same spot of the sample surface. However, the major difficulty of the suggested experiment originates in the enormous nonlinearity of the interaction process as atomic kinetics varies considerably with local energy density. Consequently, as the intensity profile of the pump x-ray beam is not uniform, each part of the exposed sample region will respond differently. This, in fact, prevents the use of a monocrystalline silicon target since the Bragg reflection will consist of unequal contributions from the entire exposed volume, therefore making analysis very difficult. In order to overcome this issue, we propose using powder samples with a well-defined grain size (tailored to the beam size, divergence, penetration depth, and bandwidth) such that the maximum possible but spatially separated number of Bragg reflections is observed at the detector. Since a typical grain size is a few-tens of microns, the grains represent an ensemble of bulk Si samples. As the powder sample homogenously fills the interaction volume, different Bragg peaks correspond to different energy densities delivered by the pump to each particular grain. Appropriate data analysis, tracking every particular Bragg reflection, combined with accurate beam profile characterization and preexposure referencing make it possible to analyze the atomic kinetics as a function of time (delay) and local pump intensity (energy density) at each particular grain.

In conclusion, we have demonstrated theoretically that in femtosecond XFEL irradiated silicon, nonthermal effects resulting in softening of the interatomic potential are visible in the stretching of oscillations of diffraction peaks as a function of fluence (or the absorbed dose). Thermal vs nonthermal melting can be identified by the absence or presence of the changes in the oscillation periods of the coherent phonons reflected in the diffraction peaks. Thus, we conclude that an experimentum crucis is possible with currently available XFELs, which would allow discriminating thermal phase transitions from nonthermal occurrences.

The authors gratefully acknowledge financial support from the Czech Ministry of Education, Youth and Sports (Grants No. LTT17015, No. EF16_013/0001552, and No. LM2015083) and from the Czech Science Foundation (Grant No. 17-05167S).

[1] C. V. Shank, R. Yen, and C. Hirlimann, Phys. Rev. Lett. **50**, 454 (1983).
[2] H. W. K. Tom, G. D. Aumiller, and C. H. Brito-Cruz, Phys. Rev. Lett. **60**, 1438 (1988).
[3] P. Stampfli and K. H. Bennemann, Phys. Rev. B **42**, 7163 (1990).
[4] P. Stampfli and K. H. Bennemann, Phys. Rev. B **46**, 10686 (1992).
[5] Y. Siegal, E. N. Glezer, L. Huang, and E. Mazur, Annu. Rev. Mater. Sci. **25**, 223 (1995).
[6] B. Rethfeld, D. S. Ivanov, M. E. Garcia, and S. I. Anisimov, J. Phys. D: Appl. Phys. **50**, 193001 (2017).
[7] E. G. Gamaly and A. V Rode, New J. Phys. **15**, 013035 (2013).
[8] T. Zier, E. S. Zijlstra, A. Kalitsov, I. Theodonis, and M. E. Garcia, Struct. Dyn. (Melville, NY) **2**, 054101 (2015).
[9] C. Lian, S. B. Zhang, and S. Meng, Phys. Rev. B **94**, 184310 (2016).
[10] K. Sokolowski-Tinten, J. Bialkowski, M. Boing, A. Cavalleri, and D. von der Linde, Phys. Rev. B **58**, R11805 (1998).
[11] A. Rousse, C. Rischel, S. Fourmaux, I. Uschmann, S. Sebban, G. Grillon, P. Balcou, E. Förster, J. P. Geindre, P. Audebert, J. C. Gauthier, and D. Hulin, Nature (London) **410**, 65 (2001).
[12] E. S. Zijlstra, J. Walkenhorst, and M. E. Garcia, Phys. Rev. Lett. **101**, 135701 (2008).
[13] N. Medvedev, Z. Li, and B. Ziaja, Phys. Rev. B **91**, 054113 (2015).
[14] I. Inoue, Y. Inubushi, T. Sato, K. Tono, T. Katayama, T. Kameshima, K. Ogawa, T. Togashi, S. Owada, Y. Amemiya, T. Tanaka, T. Hara, and M. Yabashi, Proc. Natl. Acad. Sci. USA **113**, 1492 (2016).
[15] T. Pardini, J. Alameda, A. Aquila, S. Boutet, T. Decker, A. E. Gleason, S. Guillet, P. Hamilton, M. Hayes, R. Hill, J. Koglin, B. Kozioziemski, J. Robinson, K. Sokolowski-Tinten, R. Soufli, and S. P. Hau-Riege, Phys. Rev. Lett. **120**, 265701 (2018).
[16] N. Medvedev, V. Tkachenko, V. Lipp, Z. Li, and B. Ziaja, 4open **1**, 3 (2018).
[17] *The European X-ray Free-electron Laser Technical Design Report*, edited by M. Altarelli, R. Brinkmann, M. Chergui, W. Decking, B. Dobson, S. Düsterer, G. Grübel, W. Graeff, H. Graafsma, J. Hajdu, J. Marangos, J. Pflüger, H. Redlin, D. Riley, I. Robinson, J. Rossbach, A. Schwarz, K. Tiedtke, T. Tschentscher, I. Vartaniants, H. Wabnitz, H. Weise, R. Wichmann, K. Witte, A. Wolf, and M. Wulff (DESY XFEL Project Group European XFEL Project Team Deutsches

Elektronen-Synchrotron Member of the Helmholtz Association, Hamburg, Germany, 2007).
[18] N. Medvedev, Appl. Phys. B **118**, 417 (2015).
[19] N. Medvedev, Z. Li, V. Tkachenko, and B. Ziaja, Phys. Rev. B **95**, 014309 (2017).
[20] E. S. Zijlstra, A. Kalitsov, T. Zier, and M. E. Garcia, Phys. Rev. X **3**, 011005 (2013).
[21] N. S. Grigoryan, E. S. Zijlstra, and M. E. Garcia, New J. Phys. **16**, 013002 (2014).
[22] N. Medvedev, H. O. Jeschke, and B. Ziaja, New J. Phys. **15**, 015016 (2013).
[23] H. J. Zeiger, J. Vidal, T. K. Cheng, E. P. Ippen, G. Dresselhaus, and M. S. Dresselhaus, Phys. Rev. B **45**, 768 (1992).
[24] K. Sokolowski-Tinten, C. Blome, J. Blums, A. Cavalleri, C. Dietrich, A. Tarasevitch, I. Uschmann, E. Förster, M. Kammler, M. Horn-von-Hoegen, and D. von der Linde, Nature (London) **422**, 287 (2003).
[25] T. Henighan, M. Trigo, M. Chollet, J. N. Clark, S. Fahy, J. M. Glownia, M. P. Jiang, M. Kozina, H. Liu, S. Song, D. Zhu, and D. A. Reis, Phys. Rev. B **94**, 020302 (2016).
[26] D. M. Fritz, D. A. Reis, B. Adams, R. A. Akre, J. Arthur, C. Blome, P. H. Bucksbaum, A. L. Cavalieri, S. Engemann, S. Fahy, R. W. Falcone, P. H. Fuoss, K. J. Gaffney, M. J. George, J. Hajdu, M. P. Hertlein, P. B. Hillyard, M. Horn-von Hoegen, M. Kammler, J. Kaspar, R. Kienberger, P. Krejcik, S. H. Lee, A. M. Lindenberg, B. McFarland, D. Meyer, T. Montagne, E. D. Murray, A. J. Nelson, M. Nicoul, R. Pahl, J. Rudati, H. Schlarb, D. P. Siddons, K. Sokolowski-Tinten, T. Tschentscher, D. von der Linde, and J. B. Hastings, Science **315**, 633 (2007).
[27] R. Mitzner, M. Neeb, T. Noll, N. Pontius, and W. Eberhardt, in *Proc. SPIE*, edited by Z. Chang, J.-C. Kieffer, J. B. Hastings, S. Kleinfelder, and D. L. Paisley (International Society for Optics and Photonics, 2005), p. 59200D.
[28] R. Mitzner, B. Siemer, M. Neeb, T. Noll, F. Siewert, S. Roling, M. Rutkowski, A. A. Sorokin, M. Richter, P. Juranic, K. Tiedtke, J. Feldhaus, W. Eberhardt, and H. Zacharias, Opt. Express **16**, 19909 (2008).
[29] S. Roling, V. Kärcher, L. Samoylova, K. Appel, S. Braun, P. Gawlitza, F. Siewert, U. Zastrau, M. Rollnik, F. Wahlert, and H. Zacharias, in *Proc. SPIE*, edited by T. Tschentscher and L. Patthey (International Society for Optics and Photonics, 2017), p. 1023713.
[30] J. Sakamoto, K. Ohwada, M. Ishino, J. Mizuki, M. Ando, and K. Namikawa, J. Synchrotron Radiat. **24**, 95 (2017).